Contemporary Mathematics
https://ojs.wiserpub.com/index.php/CM/

Research Article

Influence of Reaction Kinetics on Magneto-Convective Flow Through Poro-Elastic Media with Nonlinear Thermal Radiation and Buoyancy Effects

Samuel O Adesanya[1,2], Adeniyi S Onanaye[1], Ramoshweu S Lebelo[3*]

[1] Department of Mathematics and Statistics, Redeemer's University, Ede, Nigeria
[2] Education Department, Vaal University of Technology, Private Bag X021, Vanderbijlpark, 1911, South Africa
[3] Appled Physical Sciences Department, Vaal University of Technology, Private Bag X021, Vanderbijlpark, 1911, South Africa
E-mail: sollyl@vut.ac.za

Received: 7 May 2025; **Revised:** 8 July 2025; **Accepted:** 9 July 2025

Abstract: The influence of Arrhenius kinetics on magneto-convective flows in regulating temperature variation within the poro-elastic medium in several thermal, industrial, and engineering applications, such as the control of the hot molten, formation of crystals, cooling of nuclear reactors, filtration, and many more, is investigated in the present study. The exothermic nature of the chemical reaction based on Arrhenius, Sensitized, and Bimolecular kinetics suggests nonlinear heat and mass transfer. In this regard, governing equations are formulated for solid displacement in porous materials, fluid flow velocity, energy, and concentration with appropriate boundary conditions. Numerical solutions for nonlinear coupled dimensionless boundary value problems are obtained using the Spectral Chebyshev Collocation Method (SCCM) and Spectral Quasi-Linearization Method (SQLM). The two solutions are shown to be convergent. The results are further validated through the fourth-order Shooting-Runge-Kutta Scheme and presented in graphical and tabular forms. The significant contribution to knowledge in the present study reveals that the reaction parameter is an increasing function of solid displacement, flow velocity, temperature, and concentration. Similarly, increasing fluid activation energy and buoyancy values encourage solid displacement, maximum flow velocity, and temperature distribution within the flow channel while decreasing nanoparticle concentration.

***Keywords*:** reactive fluids, Jeffery liquid, spectral methods, deformable porous medium, nonlinear convection

MSC: 76S05, 76W05, 76A05

Abbreviation

(v, V)	Dimensional (m) and dimensionless axial velocity
(u, U)	Dimensional (m) and dimensionless solid displacement of porous materials
K	Flow drag force coefficient
μ_a	Lame constant
P	Fluid Pressure (Kg/ms^2)

DOI: https://doi.org/10.37256/cm.6520257201

λ_1	Retardation/relaxation time
(x, y)	Cartesian Coordinate
σ	Electrical conductivity (s/m) of Jeffery fluid
k_0	Thermal conductivity (W/mK)
B_0	Magnetic field intensity
ρ	Density of the fluid (Kg/m^3)
T, C	Dimensional Fluid temperature and concentration
θ, ϕ	Non-Dimensional Fluid temperature and concentration
β_{T_0}, β_{T_1}	Volumetric expansion due to temperature difference
T_0, T_1	Temperature at the walls (K)
β_{C_0}, β_{C_1}	Volumetric expansion due to concentration difference (1/K)
C_0, C_1	Concentration at the walls
g	Gravitational acceleration
σ^*	Stephan-Boltzmann constant
k^*	Mean absorption coefficient
D	Diffusion coefficient
α	Thermal radiation variation coefficient
ε	Activation energy parameter
Br	Brinkman number
R	Radiation parameter
$\sigma_{1,2}$	Coefficients of nonlinear buoyancies
Gr	Grashof number due to temperature difference
Gc	Grashof number due to concentration difference
M	Hartmann number
A	Rate constant
m	Reaction index
E	Activation energy (J/mol)
R	Universal gas constant
h	Channel half width (m)

1. Introduction

Appreciable progress has been reported in recent decades in studying the flow and heat transfer of viscoelastic nanofluid in deformable porous media due to its numerous applications in pharmaceuticals, biomedical fields, and engineering. Deformation of porous materials is commonly observed in medicine, geosciences, energy storage, and filtration processes. In this regard, Mallikarjuna et al. [1] utilized the Jeffrey constitutive model to study the non-Newtonian flow properties of fluid undergoing convective heat transfer and thermal radiation. In [2], Srinivas et al. reported a point collocation solution based on the Chebyshev trial function for convective flow in a poro-elastic medium. Pirhadi et al. [3] presented a finite element approach to modeling and simulating hydrocarbon recovery in a thermo-poro-elastic medium. Chen et al. [4] reported the compressible flow characteristics in fractured coals due to deformation. The study by Sreenadh et al. [5] reported the exact solution to the Couette flow model for a two-phase hydromagnetic fluid through a horizontal channel. Murthy et al. [6] highlighted the combined influence of fluid slippage, nanofluid, and Casson effect on the flow through a deformable porous medium using a numerical approach. Neeraja et al. [7] studied the importance of the additional heat source from the dense interaction of fluid particles and Newtonian cooling on the temperature and concentration of nanoparticles distribution on the Casson fluid flowing steadily down the inclined channel using shooting techniques. Castro et al. [8] investigated the characteristics of steady and oscillatory flows of Newtonian fluid through deformable porous aquifers, highlighting that the Darcy viscosity declines with injection pressure in the deformable porous medium. Recently, Sreenadh et al. [9] discussed the Newtonian fluid flow in an inclined channel

between two deformable porous layers, noting that the solid displacement increases with the angle of inclination. In contrast, it decreases with the volume fraction of the fluid. Other related studies on flows through deformable porous medium are not limited to [10–17] and the references cited in the work.

In the real sense, the linear dependence of density on temperature breaks down in several real-life cases experiencing high temperature and concentration differences. A few instances in mind can be seen in highly exothermic reactive fluids, chemotherapy and hyperthermia [18, 19], oil-recovery by combustion in geosciences, and more. Based on this fact, a nonlinear Bousinesq approximation for heat and mass transfer is expected to describe the flow behavior adequately. According to the literature, quite a good number of studies have considered nonlinear buoyancy in diverse geometries. For instance, Ganesh et al. [19] investigated Casson fluid's flow, heat, and mass transfer over a stretching surface in a porous medium with a non-uniform heat source. Qayyum et al. [20] present a homotopy analysis approximation to nonlinear heat and mass transfer of a thixotropic experiencing Newton's cooling laws. In the work of Patil et al. [21], the SQLM and finite difference approximation to Williamson fluid flowing over a rough cone in the boundary layer limit was reported. Farooq et al. [22] studied the peristaltic flow through a complaint tube exposed to nonlinear convective forces. Adeyemo et al. [23] documented the entropy generation pattern in the flow of a couple of stress fluids undergoing nonlinear convection and convective heating using SQLM approximations. The study by Xia et al. [24] addressed the multiple slippages connected to reactive hybrid nanofluid.

From a flow chemistry viewpoint, the flow of reactive fluids has many applications in oil refineries, polymerization, filtration, and other industrial procedures involving the pumping of reactive fluid in a flow channel under controlled flow rates. Given these essential applications, Jha et al. [25] studied the convective heat transfer to a reactive liquid through a uniform vertical tube subjected to Arrhenius kinetics. The steady and unsteady flow regime solutions were constructed using a small parameter analytical method and finite difference approximations since the system is nonlinear. Moreover, Kareem and Gbadeyan [26] reported that heat irreversibility is inherent in the explosive flow of hydromagnetic liquids that experience a two-step chemical reaction. Salawu et al. [27] examined the reactive flow of hybridized Williamson fluid. Their analysis includes thermal stability, ensuring the safety of the working environment. Raju et al. [28] examined the Darcian boundary layer flow, heat, and mass transfer of combustible Maxwell liquid. Ojumeri and Hamzat [29] described the magneto-hydrodynamics of reactive fluid flowing steadily through a micro-channel. Other exciting research works include studies in [30, 31] and cited references.

Motivated by the work done on the effect of exothermic chemical reactions on the magnetoconvective flow in a square cavity [32]. The main objective of this study is to investigate the combined influence of exothermic chemical reactions, nonlinear buoyancy, and radiation on the flow, heat, and mass transfer of Jeffery fluid through a deformable porous medium. The present investigation has a lot of applications in poro-elastic medium. For example, polymerization, biotechnology, chemical reactors, filtration, chemical fractionalization, and other continuous flow processes in wet sciences, where flow rate plays a vital role in the porous medium. In the next section, the problem will be formulated and non-dimensionalized, while in section three, spectral methods will be used to get the approximate solutions to the nonlinear problem. Section four is for the graphical and tabular presentation of the numerical results with appropriate explanations, while section five is for concluding remarks.

1.1 *Model formulation*

This study considers the steady convective flow of an electrically conducting, reactive Jeffrey fluid between vertical parallel plates saturated with an elastic porous material. The fluid velocity, temperature, and concentration are assumed to be constant at the walls, with no fluid slippage or temperature jump allowed. The Jeffery fluid is further assumed to undergo an exothermic chemical reaction with enormous heat radiation and nonlinear heat and mass transfer; therefore, the linearized Rosseland approximation does not apply in this case. Using the Cartesian coordinates $(x,\ y)$ as shown in Figure 1. The channel walls are assumed to be impervious, preventing fluid penetration.

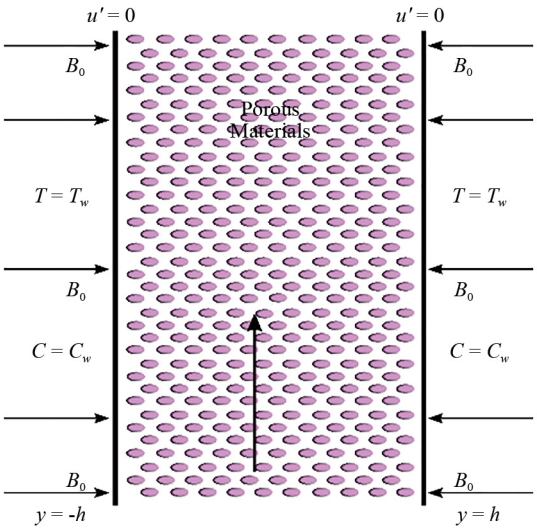

Figure 1. Flow geometry

As a result, by incorporating the nonlinear convective terms and chemical reaction, the solid displacement equation and its boundary conditions can be written as [1]

$$\mu \frac{d^2U}{dY^2} - (1-\kappa)\frac{dP}{dX} + KV = 0, U(\pm h) = 0 \tag{1}$$

Also, including the quadratic approximation into concentration, momentum equation with be boundary conditions, we get

$$\begin{aligned} &\frac{2\mu_a}{1+\lambda_1}\frac{d^2V}{dY^2} - \kappa\frac{dP}{dX} - KV - \sigma B_0^2 V + \rho g \beta_{T_0}(T-T_0) \\ &+ \rho g \beta_{T_1}(T-T_0)^2 + \rho g \beta_{C_0}(C-C_0) + \rho g \beta_{C_1}(C-C_0)^2 = 0,\ V(\pm h) = 0 \end{aligned} \tag{2}$$

The energy equation is given by

$$k_0 \frac{d^2T}{dY^2} + \frac{2\mu_a}{1+\lambda_1}\left(\frac{dV}{dY}\right)^2 + \left(K + \sigma B_0^2\right)V^2 + \frac{d}{dY}\left(\frac{4\sigma^*}{3K^*}\frac{dT^4}{dY}\right) = 0,\ T(\pm h) = T_1 \tag{3}$$

While the concentration equation with the activation energy is given by

$$D\frac{d^2C}{dY^2} - A(C-C_0)\left(\frac{T}{T_0}\right)^m e^{-\frac{E}{RT}} = 0,\ C(\pm h) = C_1 \tag{4}$$

Additional terms in equations (2) and (3) are contributions due to the reactive nature of the fluid and nonlinear double diffusivity [33, 34].

The following dimensionless parameters and variables have been adopted to convert dimensional equations into non-dimensional form

$$\left.\begin{aligned} &y=\frac{Y}{h},\ x=\frac{X}{h},\ v=\frac{V}{V_0},\ u=\frac{U}{U_0},\ \theta=\frac{E\left(T-T_0\right)}{RT_0^2},\ p=\frac{hP}{\mu_a V_0},\ \varepsilon=\frac{RT_0}{E} \\ &M^2=\frac{\sigma B_0^2 h^2}{\mu_a},\ \delta=\frac{Kh^2}{\mu_a},\ \phi=\frac{C-C_0}{C_1-C_0},\ Gc=\frac{\rho g \beta_{C_0} h^2\left(C_w-C_0\right)}{\mu_a V_0},\ Br=\frac{E}{RT_0^2}\frac{\mu_a V_0^2}{k_0} \\ &Gr=\frac{\rho g \beta_{T_0} h^2}{\mu_a V_0}\frac{RT_0^2}{E},\ \sigma_1=\frac{\beta_{T_1}}{\beta_{T_0}}\frac{RT_0^2}{E},\ \sigma_2=\frac{\beta_{C_1}}{\beta_{C_0}}\left(C_w-C_0\right),\ R=\frac{4\sigma^* T_0^3}{k^* k_0} \end{aligned}\right\} \tag{5}$$

We get

$$\left.\begin{aligned} &\frac{d^2u}{dy^2}-(1-\kappa)\frac{dp}{dx}+\delta^2 v=0, && u(\pm1)=0 \\ &\frac{2}{1+\lambda_1}\frac{d^2v}{dy^2}-\kappa\frac{dp}{dx}-\left(\delta^2+M^2\right)v+Gr\theta\left(1+\sigma_1\theta\right)+Gc\phi\left(1+\sigma_2\phi\right)=0, && v(\pm1)=0 \\ &\frac{d^2\theta}{dy^2}+Br\left(\frac{2}{1+\lambda_1}\left(\frac{dv}{dy}\right)^2+\left(\delta^2+M^2\right)v^2\right)+R\left(\frac{4}{3}(1+\alpha\theta)^3\frac{d^2\theta}{dy^2}+4\alpha(1+\alpha\theta)^2\left(\frac{d\theta}{dy}\right)^2\right)=0, && \theta(\pm1)=1 \\ &\frac{d^2\phi}{dy^2}-Kr\phi(1+\varepsilon\theta)^m e^{\frac{\theta}{1+\varepsilon\theta}}=0, && \phi(\pm1)=1 \end{aligned}\right\} \tag{6}$$

Kindly refer to the comprehensive list of nomenclature arising from equations (1)-(6) in this study. It is easy to see that in the limiting case, when equation (6) reduces to the problem solved in [1]. In the next section, the approximate solutions of the nonlinear coupled boundary value problem (6) will be obtained using spectral methods, that is, the spectral collocation method with Chebyshev polynomial as the basis function and the spectral Quasi-linearization method. The solutions obtained will be validated by the shooting-Runge-Kutta method.

2. Materials and methods

Spectral Chebyshev Collocation Method of Solution

Let us assume an admissible solution in the form of the Chebyshev polynomial $\Phi_j(y)$ as a sum of $N+1$ in which

$$\left.\begin{aligned} &u(y)\approx u^N(y)=\sum_{j=0}^{N_P}a_j\Phi_j(y),\ v(y)\approx v^N(y)=\sum_{j=0}^{N_P}b_j\Phi_j(y) \\ &\theta(y)\approx\theta^N(y)=\sum_{j=0}^{N_P}c_j\Phi_j(y),\ \phi(y)\approx\phi^N(y)=\sum_{j=0}^{N_P}d_j\Phi_j(y). \end{aligned}\right\} \tag{7}$$

with $(a_j,\ b_j,\ c_j,\ d_j)$ as coefficients to be calculated using the associated boundary conditions given in (6), then the residues can be written as:

$$
\begin{aligned}
R_1 &= u_{yy}^N - (1-\kappa)\frac{dp}{dx} + \delta^2 v^N \\
R_2 &= \frac{v_{yy}^N}{1+\lambda_1} - \kappa\frac{dp}{dx} - \left(\delta^2 + M^2\right) v^N + Gr\theta^N\left(1+\sigma_1\theta^N\right) + Gc\phi^N\left(1+\sigma_2\phi^N\right) \\
R_3 &= \theta_{yy}^N + Br\left(\frac{2}{1+\lambda_1}v_{yy}^{2N} + \left(\delta^2+M^2\right)v^2\right)v^{2N} + R\left(\frac{4}{3}\left(1+\varepsilon\theta^N\right)^3\theta_{yy}^N + 4\varepsilon\left(1+\varepsilon\theta^N\right)^2\theta_y^{2N}\right) \\
R_4 &= \phi_{yy}^N - Kr\phi^N\left(1+\varepsilon\theta^N\right)^m e^{\frac{\theta^N}{1+\varepsilon\theta^N}}
\end{aligned}
\tag{8}
$$

together with

$$
u^N(\pm 1) = 0,\ \theta^N(\pm 1) = \theta_W,\ \phi^N(\pm 1) = 1 \tag{9}
$$

The coupled system (8) is equated to zero to achieve vanishing residuals with the use of the Gauss-Lobato points, given by

$$
y_j = \cos\left(\frac{j\pi}{Np}\right), \quad j = 0,\ 1,\ 2,\ \ldots,\ N \tag{10}
$$

The equations (7)-(10) are then coded in Mathematica 13.3 for a straightforward computation. The numerical results are shown in Table 1 in the Results and Discussion section.

Spectral quasilinearization method of solution

For the problem to be solved with the spectral Quasilinearization method. We assume an approximate solution in the form $u_r,\ v_r,\ \theta_r,\ \phi_r$ for the coupled problem and the prescribed boundary conditions given in Eq. (6). Then, the quasi-linearized form of the dimensionless problem can be written as:

$$
\begin{aligned}
R_1 &= a_{0r}u_r'' + a_{1r}u_r' + a_{2r}u_r - \left(\delta^2 v_r - (1-\kappa)P + u_r''\right) \\
R_2 &= b_{0r}v_r'' + b_{1r}v_r' + b_{2r}v_r - \left(_r + Gr\theta_r\left(1+\sigma_1\theta_r\right) + Gc\phi_r\left(1+\sigma_2\phi_r\right) - \kappa P - \left(M^2+\delta^2\right)v + \frac{2u_r''}{1+\lambda_1}\right) \\
R_3 &= c_{0r}\theta_r'' + c_{1r}\theta_r' + c_{2r}\theta_r - \left(Br\left(\left(M^2+\delta^2\right)v_r^2 + \frac{2v_r'^2}{1+\lambda_1}\right) + R\left(4\varepsilon\left(1+\varepsilon\theta_r\right)^2\theta_r'^2 + \frac{4}{3}\left(1+\varepsilon\theta_r\right)^3\theta_r''\right)\right) \\
R_4 &= d_{0r}\phi_r'' + d_{1r}\phi_r' + d_{2r}\phi_r - \left(\phi_r'' - Kr\phi_r\left(1+\varepsilon\theta_r\right)^m e^{\frac{\theta_r}{1+\varepsilon\theta_r}}\right).
\end{aligned}
\tag{11}
$$

Here,

$$a_{0r}=1,\ a_{1r}=0,\ a_{2r}=0,\ b_{0r}=\frac{2}{1+\lambda_1},\ b_{1r}=0,\ b_{2r}=-\left(M^2+\delta^2\right),$$

$$c_{0r}=1+\frac{4}{3}R(1+\varepsilon\theta_r)^3,\ c_{1r}=8R\varepsilon\,(1+\varepsilon\theta_r)^2\,\theta_r',\ c_{2r}=8R\varepsilon^2\,(1+\varepsilon\theta_r)\,\theta_r'^2+4R\varepsilon\,(1+\varepsilon\theta_r)^2\,\theta_r'', \tag{12}$$

$$d_{0r}=1,\ d_{1r}=0,\ d_{2r}=-Kr\,(1+\varepsilon\theta_r)^m\,e^{\frac{\theta_r}{1+\varepsilon\theta_r}}.$$

The Gauss-Lobato point for

$$y_i=\cos\left(\frac{i\pi}{Np}\right),\quad i=0,\ 1,\ 2,\ \ldots,\ N \tag{13}$$

The generated system of linear equations is solved by the spline interpolation method using Mathematica 13.3 symbolic package, and the numerical results are presented in the following section.

3. Results and discussion

To further validate the result, the ND Solve in Wolfram Mathematica 13.3 is also used to provide an extensive solution for flow velocity, fluid temperature distribution, solid displacement, and concentration of nanoparticles. For solution convergence, specific parameter values were used to confirm the consistency of the numerical solutions, as presented in Tables 1–4. The following parameters, adopted from the literature, are used to generate the tables and graphs: $N_p=50$, $\lambda_1=0.2$, $R=\varepsilon=\alpha=Kr=M=0.1$, $m=0.5$, $P=-1$, $Gr=1=Gc=\delta$, $\sigma_1=\sigma_2=Br=0.1$, $\kappa=0.6$. The results in Tables 1-4 revealed that three solutions converged to a unique point. Therefore, the solutions are well-behaved.

Table 1. Comparison of results for solid displacement

y	$u(y)$-SQLM	$u(y)$-SCCM	$u(y)$-SRK 4
-1.00	0	0	0
-0.75	0.193689635	0.193689635	0.193689635
-0.50	0.344523072	0.344523072	0.344523072
-0.25	0.439907415	0.439907415	0.439907415
0.00	0.472505402	0.472505402	0.472505402
0.25	0.439907415	0.439907416	0.439907415
0.50	0.344523072	0.344523072	0.344523072
0.75	0.193689635	0.193689637	0.193689635
1.00	0	0	0

Table 2. Comparison of results for flow velocity

y	$v(y)$-SQLM	$v(y)$-SCCM	$v(y)$-SRK 4
-1.00	0	0	0
-0.75	0.293404691	0.293404691	0.293404691
-0.50	0.494152712	0.494152712	0.494152712
-0.25	0.611113006	0.611113007	0.611113006
0.00	0.649522840	0.649522841	0.64952284
0.25	0.611113006	0.611113007	0.611113006
0.50	0.494152712	0.494152714	0.494152712
0.75	0.293404691	0.293404695	0.293404691
1.00	0	0	0

Table 3. Comparison of results for fluid temperature

y	$\theta(y)$-SQLM	$\theta(y)$-SCCM	$\theta(y)$-SRK 4
-1.00	0	0	0
-0.75	1.01840916	1.01840917	1.01840916
-0.50	1.02754363	1.02754364	1.02754363
-0.25	1.03167547	1.03167548	1.03167547
0.00	1.0328523	1.0328523	1.0328523
0.25	1.03167547	1.03167548	1.03167547
0.50	1.02754363	1.02754362	1.02754363
0.75	1.01840916	1.01840914	1.01840916
1.00	0	0	0

Table 4. Comparison of results for concentration

y	$\phi(y)$-SQLM	$\phi(y)$-SCCM	$\phi(y)$-SRK 4
-1.00	1	1	1
-0.75	0.94693081	0.94693081	0.94693081
-0.50	0.909527077	0.909527077	0.909527077
-0.25	0.887295464	0.887295465	0.887295464
0.00	0.879920829	0.879920829	0.879920829
0.25	0.887295464	0.887295464	0.887295464
0.50	0.909527077	0.909527076	0.909527077
0.75	0.94693081	0.94693087	0.94693081
1.00	1	0.99999996	1

With the convergence of the numerical solutions, we can then discuss the graphical solutions. Figure 2 shows the magneto-convective effect on the solid displacement due to poro-elasticity of the channel. The reduction observed in the plot of solid displacement with increasing values of the Hartmann number is due to the velocity-reducing effect of the Lorentz forces. Therefore, as the magnitude of the Hartmann number increases, flow velocity decreases, which drops the magnitude of the solid displacement. Figure 2b relates the restrictive effect of magnetic field intensity to flow velocity within the flow channel. From the dimensionless equation (3), the term $-M^2v$ is a negative definite function irrespective

of the value of the Hartmann number. The negativity alters the flow direction while the magnitude of the Hartmann number is intact, as shown in the plot. Since the velocity is a decreasing function of the Hartmann number, fluid temperature is expected to drop according to the kinetic theory of matter. On the other hand, the Joule heating is a source of heat going by $+M^2v^2$, observe from Figure 2b that the velocity maximum is small $u_{\max}(M=1) < 0.8$, therefore, for sufficiently large number of Hartmann number, $v^2 \to 0$. This simply means that heat loss dominates over the heat source. That explains the reason for the drop in fluid temperature as the Hartmann number increases. It is also noted that changes in the Hartmann number have minimal effect on the concentration of the reactive fluid.

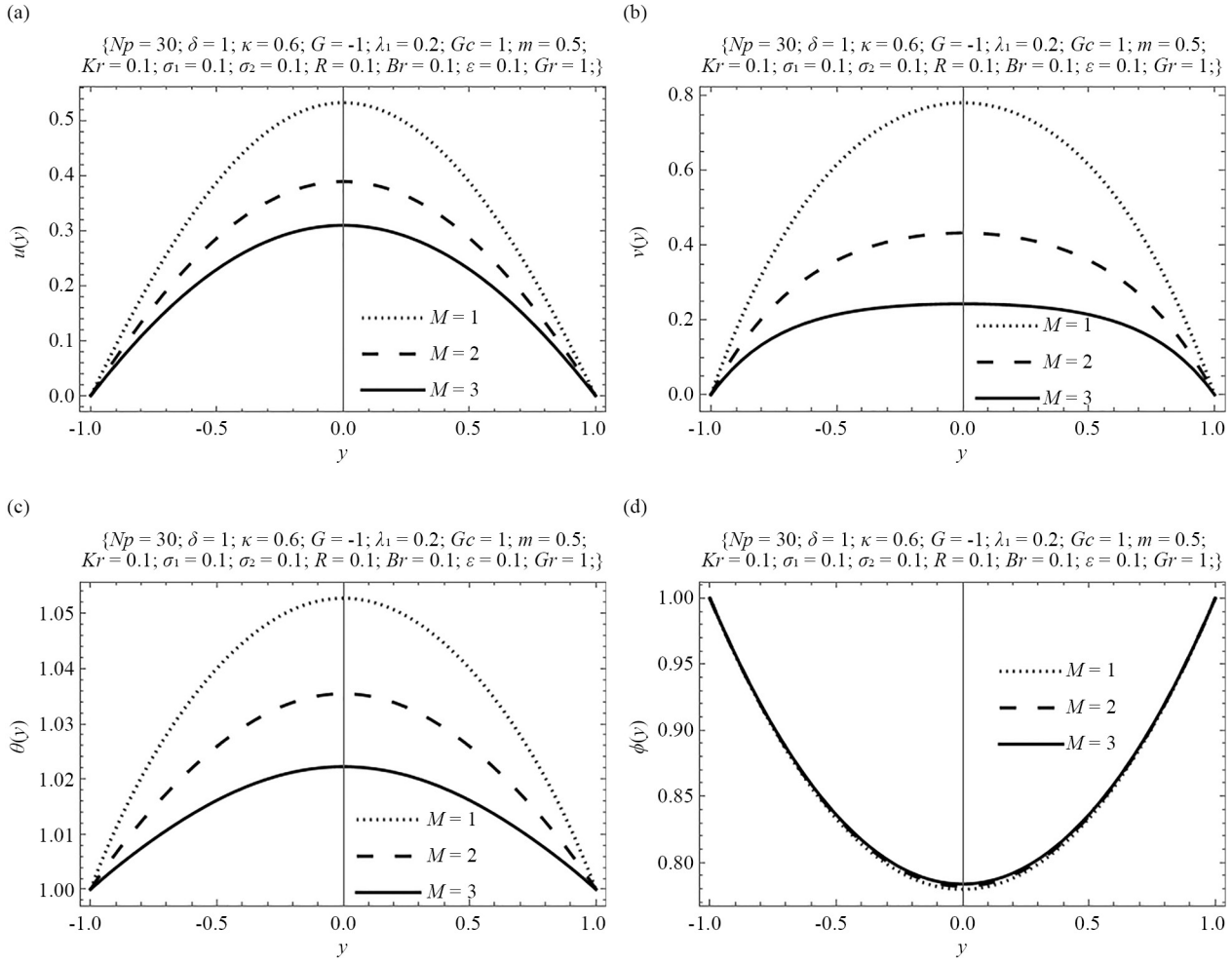

Figure 2. (a) Effect of Hartmann number on Concentration; (b) Effect of Hartmann number on velocity; (c) Effect of Hartmann number on temperature; (d) Effect of Hartmann number on Concentration

Figure 3a illustrates the effect of the Grashof number on solid displacement. The increase in solid displacement is attributed to volumetric expansion, which results from temperature differences within the flow channel. Figure 3b reveals the effect of decreasing values of activation energy requirement to induce a chemical reaction. The results indicate that as the thermal Grashof number rises, fluid velocity also increases. This effect is further emphasized in Figure 3b, which shows the influence of the Grashof number on Jeffery fluid flow. The plot reveals that a higher thermal Grashof number enhances the maximum flow velocity, likely due to heat transfer from exothermic chemical reactions. This behaviour aligns with theoretical expectations, as a lower activation energy promotes a rise in thermal Grashof number within the fluid flow. Similarly, in Figure 3b, a rise in the Grashof number heightens the fluid temperature distribution within the flow channel.

This rise is because of the synchronization between the nonlinear viscous interaction, Ohmic, and Brinkman heating of Jeffery fluid as heat sources in the flow channel. As reported in Figure 3a, 3b, 3c, increasing values of the Grashof number have increasing effects on solid displacement, Jeffery fluid velocity, and temperature. However, the concentration is meant to balance out the temperature of the fluid since temperature has a direct link with fluid concentration, but for the exponential rise in temperature, $Kr\phi(1+\varepsilon\theta)^m e^{\frac{\theta}{1+\varepsilon\theta}}$ coming from the negative definite nonlinear reaction kinetics. Expectedly, this exponential growth with increasing values of Grashof number (as reported in Figure 3c) reduces the concentration profile as observed in the plot. As explained in Figure 3d, the reaction kinetics decreases the concentration profile; this implication is reiterated in Figure 4a, in which the maximum displacement is seen at the smallest value of the control parameter, and increasing values lead to a decrease in solid displacement. A similar explanation applies to plots in 4b, 4c, and 4d. Therefore, the graphical results are well-behaved.

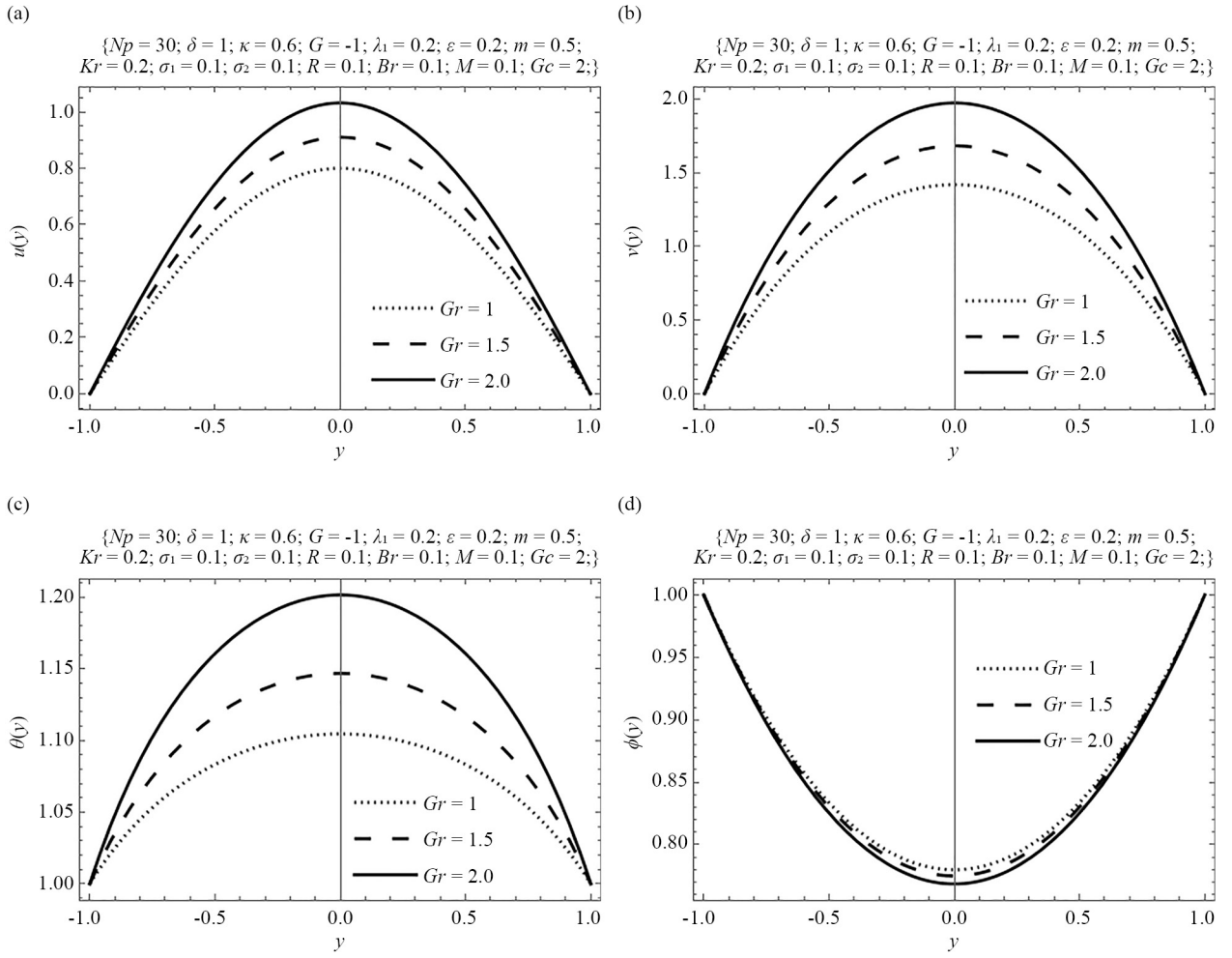

Figure 3. (a) Effect of Grashof number on displacement; (b) Effect of Grashof number on velocity; (c) Effect of Grashof number on temperature; (d) Effect of Grashof number on Concentration

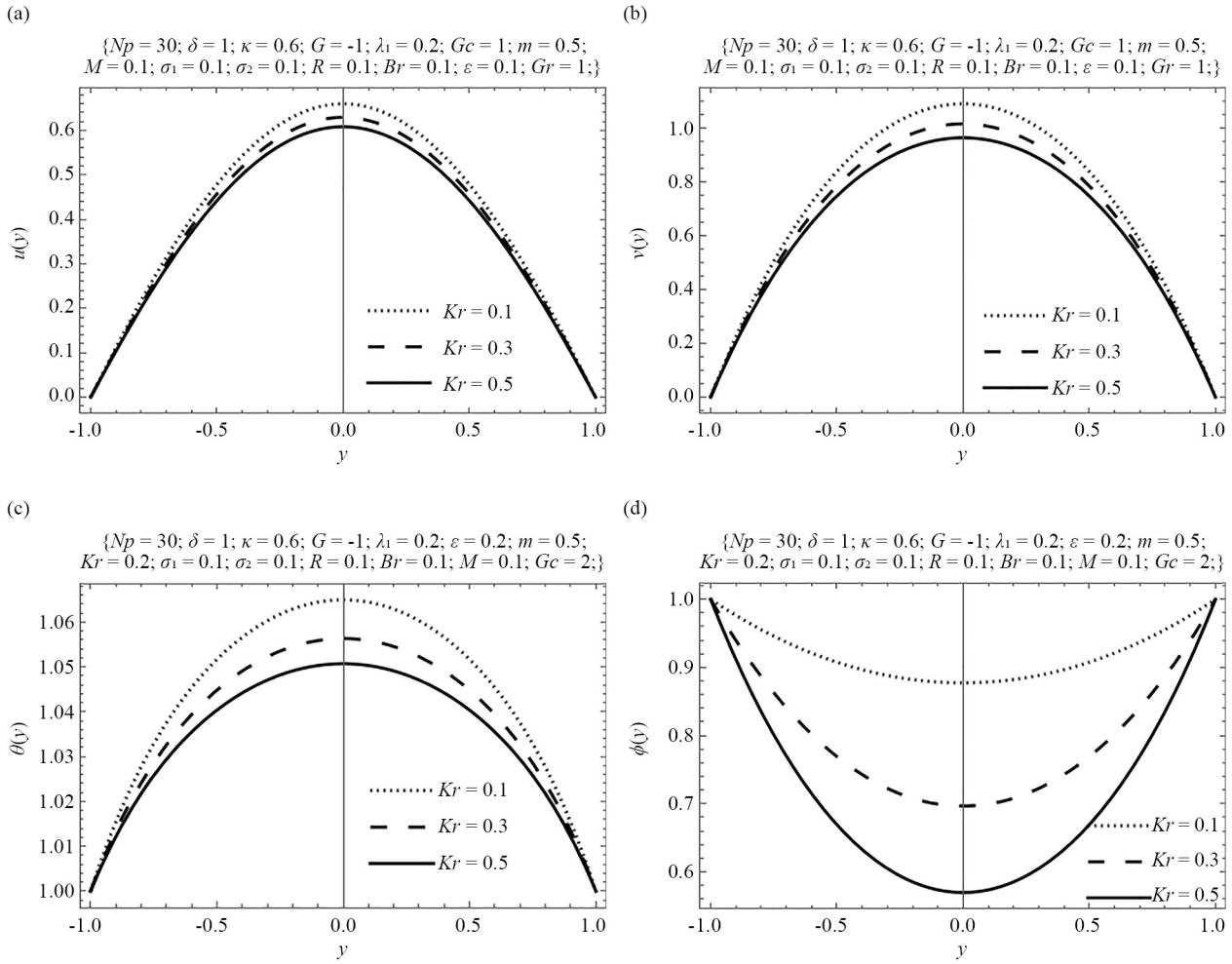

Figure 4. (a) Effect of reaction parameter on displacement; (b) Effect of reaction parameter on velocity; (c) Effect of reaction parameter on temperature; (d) Effect of reaction parameter on concentration

Figure 5a illustrates the effect of activation energy on solid displacement within a porous matrix. The plot shows that increasing the activation energy parameter reduces solid displacement, which can be attributed to the thickening of the flow. Figure 5b depicts the influence of activation energy on fluid velocity, indicating that a higher activation energy lowers the maximum flow velocity due to an increase in the viscosity of the Jeffery fluid, effectively damping the flow. In Figure 5c, the temperature profile of a bimolecular exothermic reaction reveals an inverse relationship between activation energy and fluid temperature. In other words, at high temperatures, the activation energy requirement is very low, while it requires higher activation energy at low temperatures. Finally, Figure 5a demonstrates that increasing the activation energy of the Jeffery fluid promotes an increase in fluid concentration, likely due to the reduced rate of reaction diffusion within the flow.

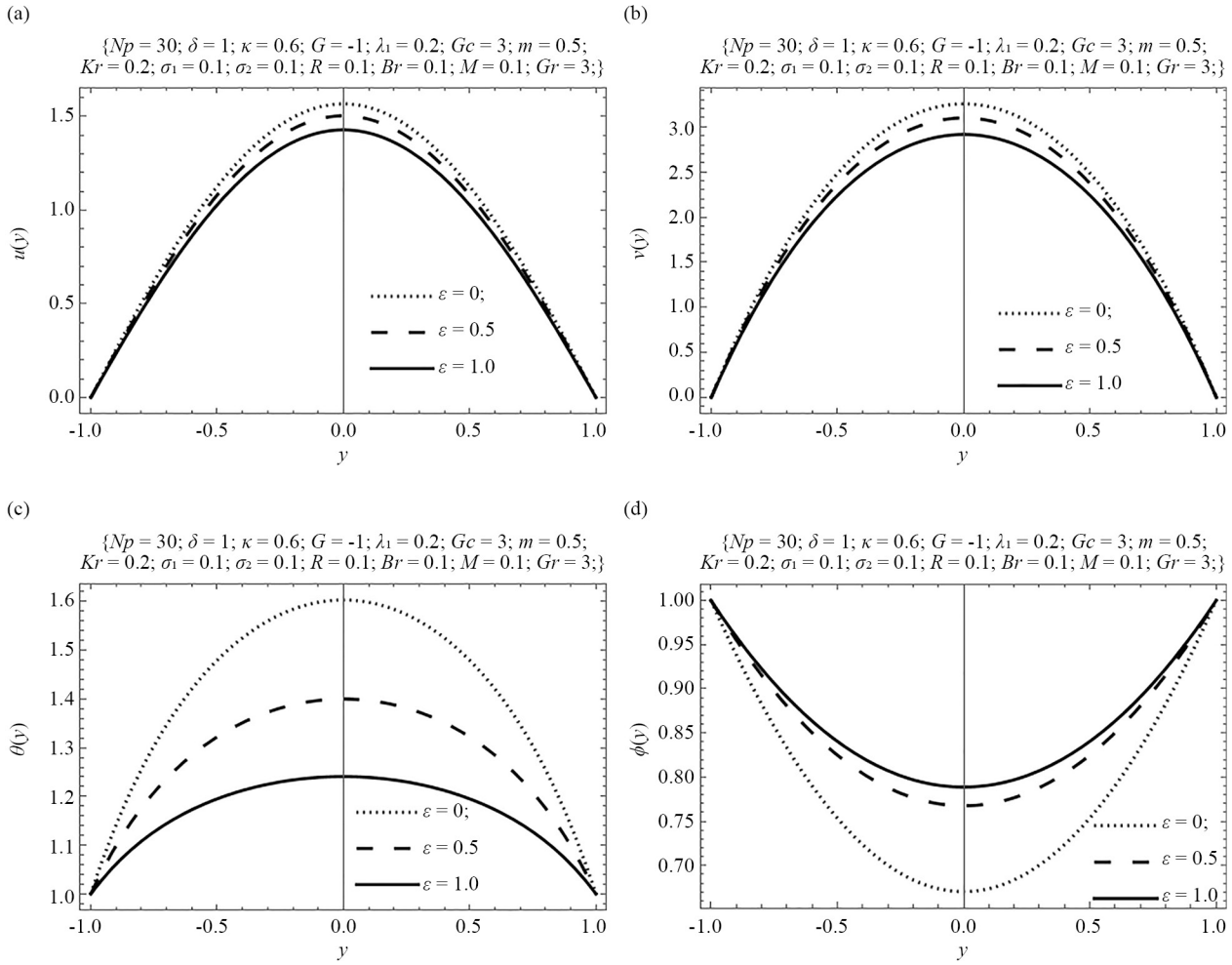

Figure 5. (a) Effect of activation energy on displacement; (b) Effect of activation energy on velocity; (c) Effect of activation energy on temperature; (d) Effect of activation energy on concentration

4. Conclusions

In the present study, the influence of exothermic chemical reaction based on Bimolecular, Arrhenius, and Sensitized kinetics on flow, heat, and mass transfer of Jeffery fluid through a deformable porous medium experiencing nonlinear thermal radiation and convection in a deformable porous medium is investigated. The channel walls are maintained at a constant wall temperature and concentration. Spectral quasi-linearization, shooting Runge-Kutta, and collocation methods are applied to obtain the approximate solutions of the dimensionless solid displacement, flow velocity, temperature and concentration. The convergence of solutions is achieved numerically and presented in tabular form. From the comparison, a good level of agreement between the methods was noticed.

The following are the major contributions to knowledge from the present study:

• A rise in the linear and quadratic Grashof numbers (thermal and solute) enhances the flow velocity, solid displacement, and temperature and lowers the concentration of the Jeffery fluid.

• The control reaction kinetics parameter decreases the magnitude of solid displacement, fluid flow, temperature, and concentration.

• Finally, an increase in the activation energy parameter results in decreased solid displacement, velocity, and temperature, while also lowering the concentration profile of the Jeffery fluid in the poro-elastic medium.

Acknowledgments

The authors express their appreciation to their respective institutions of affiliation for the administrative and other facilities they used in the course of this research work.

Conflict of interest

The authors have no competing interests to declare that are relevant to the content of this article.

References

[1] Mallikarjuna B, Srinivas J, Gopi Krishna G, Anwar Bégin O, Kadir A. Spectral numerical study of entropy generation in magneto-convective viscoelastic biofluid flow through poro-elastic media with thermal radiation and buoyancy effects. *Journal of Thermal Science and Engineering Applications*. 2022; 14(1): 011008. Available from: https://doi.org/10.1115/1.4050935.

[2] Srinivas J, Mallikarjuna B, Gopi Krishna G. Entropy generation to predict irreversibilities in poro-elastic film with multiple forces: Spectral study. *Indian Journal of Physics*. 2021; 95: 2719-2732. Available from: https://doi.org/10.1007/s12648-020-01922-0.

[3] Pirhadi A, Kianoush P, Ebrahimabadi A, Shirinabadi R. Wellbore stability in a depleted reservoir by finite element analysis of coupled thermo-poro-elastic units in an oilfield, SW Iran. *Results in Earth Sciences*. 2023; 1: 100005. Available from: https://doi.org/10.1016/j.rines.2023.100005.

[4] Chen M, Masum SA, Thomas HR. Three-dimensional cleat scale modelling of gas transport processes in deformable fractured coal reservoirs. *Gas Science and Engineering*. 2023; 110: 204901. Available from: https://doi.org/10.1016/j.jgsce.2023.204901.

[5] Sreenadh S, Prasad KV, Vaidya H, Sudhakara E, Gopi Krishna G, Krishnamurthy M. MHD Couette flow of a Jeffrey fluid over a deformable porous layer. *International Journal of Applied and Computational Mathematics*. 2017; 3: 2125-2138. Available from: https://doi.org/10.1007/s40819-016-0232-1.

[6] Krishna Murthy M. Numerical investigation on magneto-hydrodynamics flow of Casson fluid over a deformable porous layer with slip conditions. *Indian Journal of Physics*. 2020; 94: 2023-2032. Available from: https://doi.org/10.1007/s12648-019-01668-4.

[7] Neeraja A, Renuka Devi RLV, Devika B, Naga Radhika V, Krishna Murthy M. Effects of viscous dissipation and convective boundary conditions on magneto-hydrodynamics flow of Casson liquid over a deformable porous channel. *Results in Engineering*. 2019; 4: 100040. Available from: https://doi.org/10.1016/j.rineng.2019.100040.

[8] De Castro AR, Chabanon M, Goyeau B. Numerical analysis of the fluid-solid interactions during steady and oscillatory flows of non-Newtonian fluids through deformable porous media. *Chemical Engineering Research and Design*. 2023; 193: 38-53. Available from: https://doi.org/10.1016/j.cherd.2023.03.004.

[9] Sreenadha S, Uppuluri VMK, Gopi Krishna G, Srinivas ANS. Influence of thickness on porous lining when the inclined channel walls are bounded by a deformable porous layer. *International Journal of Ambient Energy*. 2024; 45(1): 2304733. Available from: https://doi.org/10.1080/01430750.2024.2304733.

[10] Sreenadh S, Gopi Krishna G, Srinivas ANS, Sudhakara E. Entropy generation analysis for MHD flow through a vertical deformable porous layer. *Journal of Porous Media*. 2018; 21(6): 523-538. Available from: https://doi.org/10.1615/JPorMedia.v21.i6.30.

[11] Eldabe NTM, Saddeek G, Elagamy K. Magneto-hydrodynamic flow of a bi-viscosity fluid through porous medium in a layer of deformable material. *Journal of Porous Media*. 2011; 14(3): 273-283. Available from: https://doi.org/10.1615/JPorMedia.v14.i3.70.

[12] Uppuluri VMK, Sreenadh S, Krishna GG. Analysis of fluid flow and entropy generation of a MHD nanofluid through a vertical channel with deformable porous medium. *Nanoscience and Technology an International Journal*. 2020; 11(3): 223-245. Available from: http://doi.org/10.1615/NanoSciTechnolIntJ.2020034777.

[13] Gopi Krishna G, Sreenadh S, Srinivas ANS. An entropy generation on viscous fluid in the inclined deformable porous medium. *Differential Equations and Dynamical Systems*. 2022; 30: 211-234. Available from: https://doi.org/10.1007/s12591-018-0411-0.

[14] Lin Y, Gopi Krishna G, Mishra SR, Ben Khedher N, Aich W, Boudjemline A, et al. Illustration of chemical reaction on the flow of viscous fluid in a deformable permeable layer: A numerical approach. *Journal of the Indian Chemical Society*. 2023; 100(2): 100875. Available from: https://doi.org/10.1016/j.jics.2022.100875.

[15] Sunil Babu G, Sreenadh S, Gopi Krishna G, Mishra S. The Couette flow of a conducting Jeffrey fluid when the walls are lined with deformable porous material. *Heat Transfer*. 2020; 49(3): 1568-1582. Available from: https://doi.org/10.1002/htj.21678.

[16] Murthy MK, Renuka Devi RLV, Swapna Y, Rachana C. Effects of multiple slip conditions on hydromagnetic flow of Jeffrey fluid over a deformable porous channel. *SN Applied Sciences*. 2019; 1: 1174. Available from: https://doi.org/10.1007/s42452-019-1183-z.

[17] Krishna Murthy M. Numerical investigation on magneto-hydrodynamics flow of Casson fluid over a deformable porous layer with slip conditions. *Indian Journal of Physics*. 2020; 94: 2023-2032. Available from: https://doi.org/10.1007/s12648-019-01668-4.

[18] Shi F, Luo D, Zhou X. Combined effects of hyperthermia and chemotherapy on the regulate autophagy of oral squamous cell carcinoma cells under a hypoxic microenvironment. *Cell Death Discovery*. 2021; 7: 227. Available from: https://doi.org/10.1038/s41420-021-00538-5.

[19] Vishnu Ganesh N, Al-Mdallal QM, Kalaivanan R, Reena K. Arrhenius kinetics driven nonlinear mixed convection flow of Casson liquid over a stretching surface in a Darcian porous medium. *Heliyon*. 2023; 9(6): e16135. Available from: https://doi.org/10.1016/j.heliyon.2023.e16135.

[20] Qayyum S, Hayat T, Alsaedi A, Ahmad B. MHD nonlinear convective flow of thixotropic nanofluid with chemical reaction and Newtonian heat and mass conditions. *Results in Physics*. 2017; 7: 2124-2133. Available from: https://doi.org/10.1016/j.rinp.2017.06.010.

[21] Patil PM, Hiremath PS, Momoniat E. Impulsive motion causes time-dependent nonlinear convective Williamson nanofluid flow across a rough conical surface: Semi-similar analysis. *Alexandria Engineering Journal*. 2023; 74: 171-185. Available from: https://doi.org/10.1016/j.aej.2023.05.023.

[22] Farooq S, Shoaib T, Bukhari SZB, Alqahtani AS, Malik MY, Abdullaev S, et al. Peristaltic motion of Jeffrey fluid with nonlinear mixed convection. *Heliyon*. 2023; 9(11): e21451. Available from: https://doi.org/10.1016/j.heliyon.2023.e21451.

[23] Adeyemo AS, Sibanda P, Goqo SP. Analysis of heat and mass transfer of a non-linear convective heat generating fluid flow in a porous medium with variable viscosity. *Scientific African*. 2024; 24: 2140. Available from: https://doi.org/10.1016/j.sciaf.2024.e02140.

[24] Xia W-F, Ahmad S, Khan MN, Ahmad H, Rehman A, Baili J, et al. Heat and mass transfer analysis of nonlinear mixed convective hybrid nanofluid flow with multiple slip boundary conditions. *Case Studies in Thermal Engineering*. 2022; 32: 101893. Available from: https://doi.org/10.1016/j.csite.2022.101893.

[25] Jha BK, Samaila AK, Ajibade AO. Transient free-convective flow of reactive viscous fluid in vertical tube. *Mathematical and Computer Modelling*. 2011; 54(11-12): 2880-2888. Available from: https://doi.org/10.1016/j.mcm.2011.07.008.

[26] Kareem RA, Gbadeyan JA. Entropy generation and thermal criticality of generalized Couette hydromagnetic flow of two-step exothermic chemical reaction in a channel. *International Journal of Thermofluids*. 2020; 5(6): 100037. Available from: https://doi.org/10.1016/j.ijft.2020.100037.

[27] Salawu SO, Obalalu AM, Shamshuddin MD, Fatunmbi EO, Ajilore OJ. Thermal stability of magneto-hybridized silicon and aluminum oxides nanoparticle in Williamson exothermic reactive fluid with thin radiation for perovskite solar power. *Kuwait Journal of Science*. 2024; 51: 100284. Available from: https://doi.org/10.1016/j.kjs.2024.100284.

[28] Raju U, Rangabashyam S, Alhazmi H, Khan I. Irreversible and reversible chemical reaction impacts on convective Maxwell fluid flow over a porous media with activation energy. *Case Studies in Thermal Engineering*. 2024; 61: 104821. Available from: https://doi.org/10.1016/j.csite.2024.104821.

[29] Ojemeri G, Hamza MM. Heat transfer analysis of Arrhenius-controlled free convective hydromagnetic flow with heat generation/absorption effect in a micro-channel. *Alexandria Engineering Journal*. 2022; 61(12): 12797-12811. Available from: https://doi.org/10.1016/j.aej.2022.06.058.

[30] Adesanya SO, Falade JA, Ukaegbu JC, Makinde OD. Adomian-Hermite-Padé approximation approach to thermal criticality for a reactive third grade fluid flow through porous medium. *Theoretical and Applied Mechanics*. 2016; 43(1): 133-144. Available from: https://doi.org/10.2298/TAM1601133A.

[31] Adesanya SO, Banjo PO, Lebelo RS. Exergy analysis for combustible third-grade fluid flow through a medium with variable electrical conductivity and porous permeability. *Mathematics*. 2023; 11: 1882. Available from: https://doi.org/10.3390/math11081882.

[32] Hasan MM, Uddin MJ, Nasrin R. Exothermic chemical reaction of magneto-convective nanofluid flow in a square cavity. *International Journal of Thermofluids*. 2022; 16: 100236. Available from: https://doi.org/10.1016/j.ijft.2022.100236.

[33] Adesanya SO, Adeosun AT, Lebelo RS, Tisdell C. Numerical investigation of reaction driven magneto-convective flow of Sisko fluid. *Numerical Heat Transfer, Part A: Applications*. 2024; 1-14. Available from: https://doi.org/10.1080/10407782.2024.2355513.

[34] Adesanya SO, Rundora L, Thosago KF. Numerical evaluation of heat irreversiblity in porous medium combustion of third-grade fluid subjected to Newtonian cooling. *Numerical Heat Transfer, Part A: Applications*. 2023; 84(9): 1091-1105. Available from: https://doi.org/10.1080/10407782.2023.2171520.